THE NORMAL MODES OF THE GRAMICIDIN-A DIMER CHANNEL

BENOIT ROUX AND MARTIN KARPLUS
Department of Chemistry, Harvard University, Cambridge, Massachusetts 02138

ABSTRACT The dynamics of the gramicidin-A dimer channel is studied in the harmonic approximation by a vibrational analysis of the atomic motions relative to their equilibrium positions. The system is represented by an empirical potential energy function, and all degrees of freedom (bonds lengths, bond angles, and torsional angles) are allowed to vary. The thermal fluctuations in the backbone dihedral angles ϕ and ψ, atomic root mean square displacements, and the correlations between the different amide planes are computed. It is found that only adjacent dihedral ψ_i and ϕ_{i+1} are strongly correlated, while different hydrogen-bonded amide planes are only weakly correlated. Modes with relatively low vibrational frequencies (75–175 cm^{-1}) make the dominant contributions to the carbonyl librations. The general flexibility of the structure and the role of carbonyl librations in the ion transport mechanism are discussed.

I. INTRODUCTION

The gramicidin-A (GA) channel is the best characterized ion selective transmembrane structure (1). Even though its natural function may not be that of a transmembrane channel, but rather as a cofactor in RNA synthesis (2), GA has proved to be an extremely useful model system for the study of the principles governing ion transport across lipid membranes. The GA channel shows a nontrivial selectivity among small monovalent cations ($Li^+ < Na^+ < K^+ < Cs^+$) and appears to be almost impermeable to anions (3). Unfortunately, due to its sensitivity to the environment, there is still no high resolution x-ray structure for the GA channel (4–6). The structure of the channel has been investigated by numerous methods, including circular dichroism (4, 7), infrared spectroscopy (8, 9), tryptophan fluorescence energy transfer (10), chemical modifications and functional measurements (11), neutron-diffraction (12), and nuclear magnetic resonance (13–20). There is now considerable evidence that the functional structure of the channel in the lipid membrane is a head-to-head dimer, each monomer being a left-handed β6.3 helix; this structure was first proposed by Urry in 1971 (4, 7). Recently, Arseniev et al. (19) have proposed that GA forms a head-to-head right-handed helix dimer in sodium dodecyl-d_{25} sulfate micelles on the basis of two-dimensional protons nuclear Overhauser effect data, and it is in fact possible that the channel structure may vary depending on the membrane environment. Most of the conductance experiments have been performed with glyceryl mono-oleate membranes and it is believed that the left-handed helical structure occurs in this environment (Urry, D. private communication).

In agreement with the available structural and ion permeability data, there have been a range of theoretical studies concerned with the GA channel. Most early analyses of ion permeability were based on Eyring-type rate theory (13, 21). This approach has contributed significantly to the characterization of the transition rates associated with ion translocation and the free energy profile of ions inside the channel. Also a number of approximate microscopic models have been proposed for the essential features of ion transport in gramicidin channels. There are gramicidin-like models, in which the channel is represented as a cylinder with certain charges or fixed carbonyl group (21–31) and more detailed atomic models of the channel (32–41). While the calculations of the ion transport properties have employed simplified models for computational reasons (see reference 27 for a review), the detailed atomic models have been used in an attempt to obtain a more realistic picture of the system. Absolute rate theory formalism (23, 26), stochastic Brownian dynamics (25, 30), molecular dynamics (23, 24, 31, 32), energy minimization (28, 34–36, 39, 40), and Monte Carlo simulations (37, 38) have all been applied to the GA channel. Most of the calculations based on detailed atomic models used a rigid or nearly rigid right-handed β6.3 helix with the structural parameters proposed by Urry. Nevertheless, it is commonly believed that the fluctuations of the channel structure play an important role in the transport process. In fact, carbonyl librations have been proposed as a mechanism to help accomodate the presence of a cation in the channel (42). The importance of the flexibility of the ethanolamine end group (EAM) has also been stressed (36). Despite their possible importance, the amplitudes and the time scales involved in the fluctuations of the GA dimer have not been fully quantified. Only the molecular dynamics simulation of Mackay et al. (32) has dealt with all degrees

of freedom, but the relatively short simulation time (5 ps) does not allow a characterization of the low frequency motions.

In this paper we investigate the fluctuations of the GA dimer in the head-to-head conformation using a normal mode analysis. In such an approach the fluctuations of the atoms around their equilibrium positions are assumed to be sufficiently small to permit approximation of the potential energy as a sum of terms that are quadratic in the Cartesian displacements. Although molecular dynamics simulations have shown that the fluctuations of macromolecules have significant anharmonic contributions (43, 44), a harmonic analysis can nevertheless provide useful insights concerning the motional behavior and flexibility (45, 46). It has the advantage relative to molecular dynamics simulations in that it gives exact results, independent of the time scales, for the assumed harmonic potential. In studies of proteins it has been noted that the harmonic approximation gives a rather reliable picture of the backbone dynamics, but that the side chain atoms tend to be more anharmonic (44, 47). This is of importance here since the ion channel of GA involves mainly the backbone atoms, with the hydrophobic side chains extending into the surrounding medium. A normal modes analysis related to the β6.3 helical structure has been reported by Naik and Krimm (8, 9), but their calculations used a simplified atomic model and approximated the molecule as an infinite polyalanine-like helix. They also focused mainly on the high frequency vibrational motions of the backbone atoms (i.e., the various amide frequencies in the 1,500 cm^{-1} range) that are thought to be diagnostic for the nature of the helical structure. Here our primary concern is with the lower frequency modes that may couple to the ion and water motions in the gramicidin channel.

Section II describes the structure of the gramicidin channel and the methods used for energy minimization and normal mode analysis. In section III we present the results. Particular attention is focussed on the low frequency motions and their contributions to atomic, carbonyl, and amide plane fluctuations. A concluding discussion is given in section IV.

II. METHOD

One monomer was built as an ideal β6.3 left-handed helix starting with the dihedral angles provided by Urry (39) (see Table I); the side chains were introduced in their extended configuration. The dimer was constructed by docking two monomers with the help of the molecular graphics program HYDRA and the resulting structure was refined by energy minimization. A special image algorithm preserving the symmetry of the dimer was used during the energy minimization, but no helical symmetry was imposed on the structure.

The force field used was that of CHARMM and has been described elsewhere (48). The energy contains terms corresponding to internal bonded interactions (bond stretching, angle bending, dihedral angle, and improper dihedral angles potential terms), and external nonbonded interactions (van der Waals and electrostatic terms). The model includes all heavy atoms and all polar hydrogens that can be involved in H-bonds; the remaining hydrogens were treated as part of the heavy atom to which they are attached (extended atom model). This leads to 157 particles in each monomer. A distance-dependent dielectric constant was used to approximate the shielding effects of the solvent, which was not included explicitly (48, 58). The minimization was terminated when the average rms force on a particle was <0.01 kcal/mol-Å.

TABLE I
DIHEDRALS ANGLES OF THE MINIMIZED GA DIMER*

Residues‡	ϕ	ψ	χ_1	χ_2
L-Val-1	−109.59	122.56	−177.28	
D-Gly-2	109.79	−110.90		
L-Ala-3	−141.97	138.97		
D-Leu-4	83.54	−131.95	−175.25	170.75
L-Ala-5	−130.89	129.33		
D-Val-6	109.38	−146.08	172.87	
L-Val-7	−120.57	116.29	−176.52	
D-Val-8	123.67	−122.03	−178.66	
L-Trp-9	−129.41	135.10	−165.72	94.11
D-Leu-10	90.67	−94.41	168.90	175.63
L-Trp-11	−146.46	135.54	171.82	58.81
D-Leu-12	80.05	−88.50	166.80	173.95
L-Trp-13	−147.22	138.29	174.92	61.54
D-Leu-14	80.24	−96.57	170.50	172.04
L-Trp-15	−153.59	120.95	−147.55	98.39

*The starting values (Urry, 1983) were $\phi = -140.0$, $\psi = +130.0$ for L-amino acids and $\phi = +100.0$, $\psi = -120.0$ for D-amino acids; the side chains were all built in the extended conformation ($\chi_1 = 180°$, $\chi_2 = 180°$.

‡The standard numbering is followed from the NH_2- to the COOH-terminal end; the mouth of the channel is at the COOH-terminal end and the dimer contact at the NH_2-terminal end.

The symmetry of the system was exploited to calculate the second derivative matrix of the potential energy of the minimized structure in block diagonal form. This corresponds to writing the matrix on the basis of symmetric and antisymmetric Cartesian displacements. The two blocks are simply constructed from the second derivative matrix elements $V_{ip,jq}$, where indices lp represent the ith Cartesian component of the pth particle, and jq represent the jth Cartesian component of the qth particle. Assuming the axis of symmetry is oriented along one of the Cartesian axis, one can write that

$$V_{ip,jq} = \lambda_i \lambda_j V_{ip',jq'} \tag{1.1}$$

and that

$$V_{ip,jq'} = \lambda_i \lambda_j V_{ip',jq}, \tag{1.2}$$

where the primed indices refer to the second monomer, and λ_i (λ_j) is +1 if the ith (jth) Cartesian component is oriented along symmetry axis, and −1 otherwise. It follows that

$$V^{SYM}_{ip,jq} = V_{ip,jq} + \lambda_i V_{ip',jq} \tag{2.1}$$

and

$$V^{ANT}_{ip,jq} = V_{ip,jq} - \lambda_i V_{ip',jq}. \tag{2.2}$$

Separate diagonalization of each of these symmetry blocs provided 471 symmetric and 471 antisymmetric normal modes. In this representation, the zero-frequency mode for rotation around the symmetry axis and the translational mode along the same axis appear in the symmetric set; the four other zero-frequency modes appear in the antisymmetric set. All the calculations were performed in mass-weighted Cartesian coordinates and the matrix diagonalization was performed with the double precision IMSL routine EIGRS.

III. RESULTS

Features of Minimized Structure

After minimization, the structure of the monomers deviated significantly from the ideal β6.3 helix. This is due to the finiteness of the chain and the interactions between the side chains. The final set of dihedral angles ϕ-ψ is shown in Table I. The alternating sequence of $(-, +)$ for L-amino acids and $(+, -)$ for D-amino acids was conserved, but there are important deviations from the initial structure. The major changes are observed for residues 10 to 15, which affect the last helix turn at the mouth of the channel. This deviation from the ideal structure was caused by the formation of two 1–7 hydrogen bonds (49) between L-Tryp 11-C=O · · · · HN-L-Trp-13 and L-Trp 13-C=O · · · · NH-L-Trp 15. The average H · · · O distance of hydrogen bond groups in the initial structure was near 2.25 Å; the final H bond distance is 1.9 Å. That of the 1–7 hydrogen H-bonds was ~3.4 Å initially, and the minimization resulted in a distance of 2.4 Å. These distortions are a direct consequence of the finiteness of the helix, although they might be reduced somewhat by the presence of solvent (49). No important change is observed in the hydrogen bond network. The ethanol amine tail is doubly hydrogen bonded to the helix (O hydroxyl · · · · HN L-Trp_{11}, and H hydroxyl · · · · O=C L-Trp_{11}). The conformation of many side chains are different from those proposed previously (39); the most noticeable change concerns the side chains of L-Trp_9 and L-Trp_{15}. This fact is not surprising because the side chains are essentially nonpolar and have considerable freedom to reorient with respect to the helical backbone of the channel. Indeed, many different side chains conformations could be found with little effort. A complete enumeration of all the possible side chains substates was not attempted. There are no experimental data on the side chain conformation, although the possibility of numerous low energy conformations has been proposed as an explanation for the many conducting states found experimentally (42). It is likely that the side chains are affected considerably by the presence of the membrane. These questions can not be addressed by a normal mode calculation restricted to one particular minimized structure. For these reasons our analysis focused mainly on the backbone fluctuations of the structure. The structure before and after energy minimization is shown in Fig. 1.

Normal Mode Analysis

The frequency spectrum of the calculated normal modes is shown in Fig. 2. The general aspect of the spectrum is very similar to those reported for proteins with analogous potential energy functions (46, 50–52). There is a broad shoulder between 50 and 200 cm^{-1}, followed by a relatively flat region of lower density of 200 to 500 cm^{-1}. At higher frequencies, the modes are dominated by independent motions such as angle bending and bond stretching. There are 120 modes in the region of the spectrum from 10 to 200 cm^{-1}. This number corresponds roughly to the 114 dihedral degrees of freedom in the GA dimer. The general features of the low-frequency normal mode spectrum of GA corresponds to that expected from a general analysis for polypeptide macromolecular systems (52).

Because the structure was not at an absolute minimum, two negative modes were found, one symmetric and one antisymmetric. They were local in character, and mainly involved the first residue of each monomer in the head-to-head region. An energy search along the lowest frequency positive modes showed significant anharmonic components only for the first few modes. The lowest frequency mode (2.8 cm^{-1}) showed the strongest anharmonicity. Its true frequency as estimated from the energy search was ~75 cm^{-1}. This mode, which is localized in the dihedral angles of residues L-Ala_5 and D-Val_6 was removed from the fluctuations analysis. In subsequent analyses, the spectrum was assumed to start with the second lowest mode (4.6 cm^{-1}). The 25 lowest symmetric and antisymmetric modes are listed in Table II.

Low Frequency Motion Analysis

The projection of the symmetric mode onto the antisymmetric modes are shown in Fig 3 *a*; the *n*th symmetric mode is projected on the *n*th antisymmetric and each projection is averaged over the 10 nearest modes to produce a smoother curve. An average overlap >0.8 is found for the modes above 75 cm^{-1}; for modes above 170 cm^{-1}, the overlap is close to unity. Fig. 3 *b* shows the frequencies of the symmetric and antisymmetric modes. Again, they appear to differ significantly only below 75 cm^{-1}. This suggests that collective modes involving interactions between the two monomers are mostly at frequencies below this cutoff.

The low frequency modes can be understood in terms of a model based on continum mechanics (Elber, R., and M. Karplus, unpublished results). For very low frequency motions, one can picture the GA dimer as a short elastic rod of length L. Such an elastic rod can have motions characterized as torsion, bending, and stretching. The equations of motions governing the motions of a elastic rod in the simplest description are (55):

$$\frac{\partial^2\theta}{\partial z^2} = A\frac{\partial^2\theta}{\partial^2 t} \tag{4a}$$

with the boundary conditions at the ends,

$$\frac{\partial\theta}{\partial z} = 0; \tag{4b}$$

bending:

$$\frac{\partial^4 b}{\partial z^4} = B\frac{\partial^2 b}{\partial^2 t} \tag{5a}$$

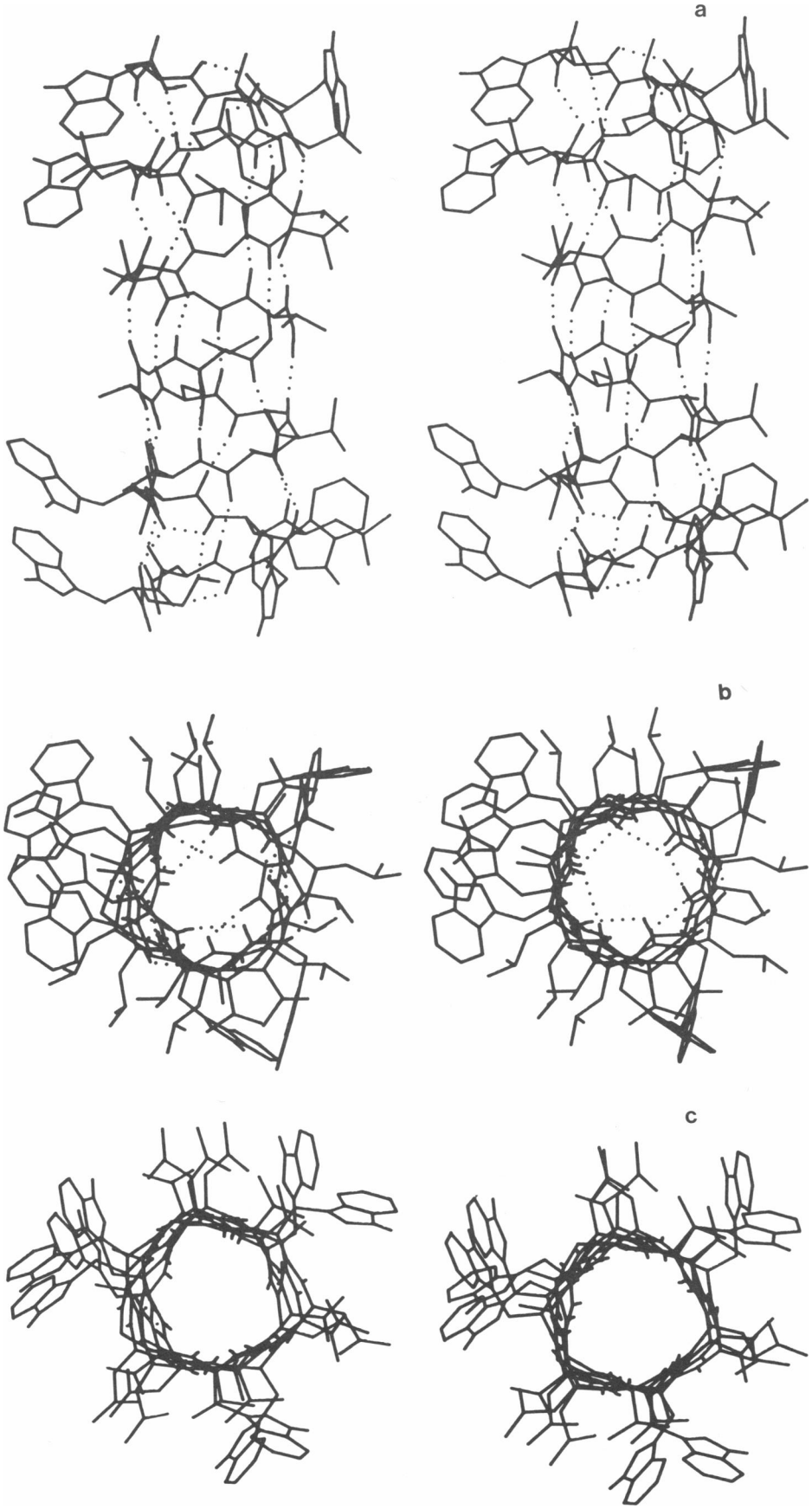

FIGURE 1 Stereo picture of the energy minimized structure of Gramicidin-A. (*a*) Energy-minimized structure with the axis of symmetry coming out of the page. (*b*) Energy minimized structure looking down the channel. (*c*) Initial structure looking down the channel.

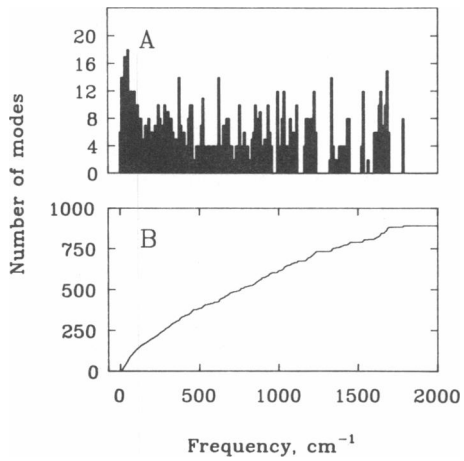

FIGURE 2 Normal modes frequencies. (*a*) Histogram of the number of normal modes per 10 cm^{-1} interval; the maximum density is equal to 18 modes and is found in the interval 50–60 cm^{-1}. (*b*) Cumulative distribution of the number of modes as a function of frequency.

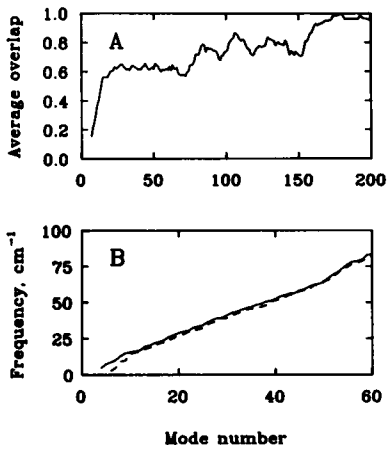

FIGURE 3 Comparison of the symmetric and the antisymmetric modes. (*a*) Projection of the symmetric modes onto the antisymmetric modes as a function of mode number. The projections are averaged over the ten nearest modes to produce a smoother curve. (*b*) Frequencies of the symmetric modes (*solid line*) and frequencies of the antisymmetric modes (*dash line*).

with the boundary condition at ends,

$$\frac{\partial^3 b}{\partial z^3} = \frac{\partial^2 b}{\partial z^2} = 0; \tag{5b}$$

stretching:

$$\frac{\partial^2 s}{\partial z^2} = C\frac{\partial^2 s}{\partial t^2} \tag{6a}$$

with the boundary condition at ends,

$$\frac{\partial s}{\partial z} = 0. \tag{6b}$$

In Eqs. (4–6), A, B, and C are constants related to Young's modulus and the various moments of inertia of the elastic rod (53), z is the coordinate along the helix axis, t is the time, $\theta(z, t)$ is the torsion angle around the helix axis, $b(z, t)$ is the bending displacement perpendicular to the helix axis, and $s(z, t)$ is the stretching displacement along the axis.

TABLE II
LOWEST FREQUENCY MODES AND THEIR SYMMETRY*

1	2.811	ANT	2	4.656	SYM
3	4.881	ANT	4	7.435	SYM
6	9.275	ANT	5	8.866	SYM
8	10.071	ANT	7	10.223	SYM
10	14.357	ANT	9	12.990	SYM
12	15.556	ANT	11	14.988	SYM
14	16.306	ANT	13	15.779	SYM
17	17.840	ANT	15	16.392	SYM
18	18.984	ANT	16	16.909	SYM
20	19.837	ANT	19	19.544	SYM
22	21.920	ANT	21	20.438	SYM
24	22.730	ANT	23	22.066	SYM
25	22.818	SYM			

*All frequencies in cm^{-1}.

All boundary conditions were applied at $\pm L/2$, where L is the length of the GA dimer (chosen to be equal to 30 Å). For each of the three types of motions, the form of normal modes of the elastic rod are determined completely by the boundary conditions given by Eqs. 4b–6b, while the frequencies are determined by both the boundary conditions and the elastic constants A, B, and C. Since we are concerned with the relation of the form of displacements of the elastic rod to the normal modes of GA, the actual value of the constants in unimportant.

The solutions of these differential equations generate three subsets of hypothetical atomic displacement vectors corresponding to "ideal" collective motions such as torsions ($\mathbf{T}_i, i = 1 \ldots$), bending ($\mathbf{B}_i, i = 1 \ldots$), and stretching ($\mathbf{S}_i, i = 1 \ldots$); the T_i are expressed in terms of $\theta(z)$, the B_i in terms of $b(z)$, and the S_i in terms of $s(z)$. The fraction of overlap between these subsets and the actual GA calculated normal models, $\mathbf{v}_k$, is given by the Euclidian inner product with the mass-weighted normalized vectors.

$$\mathbf{T}'_i = M^{1/2}\mathbf{T}_i \tag{7a}$$

$$\mathbf{B}'_i = M^{1/2}\mathbf{B}_i \tag{7b}$$

$$\mathbf{S}'_i = M^{1/2}\mathbf{S}_i \tag{7c}$$

$$\mathbf{v}'_k = M^{1/2}\mathbf{v}_k, \tag{7d}$$

where $M^{1/2}$ is the square root of the diagonal mass matrix. The normal modes obtained by solving the continuum elasticity equations are automatically orthogonal. This is no longer true when they are used to generate the displacements of a molecule consisting of discrete masses. To avoid multiple counting of overlap in the inner product, the three subsets of collective mass-weighted displacements were separately orthogonalized by the Gram-Schmidt method.

Also, since it is meaningless to include modes having a wavelength shorter than the average interatomic distance, only the first ten continuum modes in each of the three sets were included. They correspond to motions having a wavelength greater than or equal to the helix pitch, i.e., since the length of the dimer is ~30 Å, and there are six helix turns, the pitch equals ~5 Å.

The total projection of the kth normal model, $\mathbf{v}_k$ onto these subspace is defined by

$$\text{overlap}_k = \left(\sum_i (\mathbf{T}'_i \cdot \mathbf{v}'_k)^2 \right)^{1/2} \tag{8}$$

with similar expressions for the bending and the stretching motions. The calculated projections are shown in Fig. 4. It is clear that many low frequency modes can be identified with those of the continuum theory. Collective torsion and bending motions are found at frequencies lower than 30 cm^{-1}. Very few low frequency modes are pure stretching motions. The stretching modes are located at higher frequencies because stretching of the helix has a relatively large effective force constant due to the presence of hydrogen bonds (45). Analysis of the fluctuations shows that the length of the hydrogen bonds does not vary by more than 0.1 Å.

Other collective motions are expected between 30 and 75 cm^{-1}, as suggested by the comparison of the symmetric and antisymmetric normal modes (Fig. 3). However, the continuum elastic model is not valid for this frequency range and so does not allow us to draw definitive conclusions about their character.

Carbonyl Librations

The special features of the GA structure make the so-called carbonyl librations a plausible mechanism for shielding a positive ion from the low dielectric region of the lipid membrane. The loss of hydration energy when waters are stripped off as the ion enters the channel is assumed to be compensated by a slight distorsion of the channel backbone that provides a favorable interaction of the ion with some of the negatively charged carbonyl oxygens. For this suggestion to be plausible, the energy required for a libration must be sufficiently small that it is more than compensated for by the interaction with the ion. The libration mechanism of GA dimer has been discussed in numerous papers (40, 42). Libration of a transpeptide unit (amide plane between the consecutive amino acids) can be described as an almost rigid rotation of the planes (C_i, O_i, N_{i+1}, H_{i+1}) around the axis defined by the ($C^\alpha_i - C_i$) and ($N_{i+1} - C^\alpha_{i+1}$). A librational motion corresponds to a small change in the dihedral angle ψ_i to $\psi_i + \delta$, that is associated with an equal and opposite change of ϕ_{i+1} to $\phi_{i+1} - \delta$. Such anticorrelated motion of transpeptide units have been reported for other peptide helices (45). In this hypothetical motion, all C^α and side chain atoms remain more or less fixed. However, since the bonds involved are not perfectly colinear, the peptide plane libration requires some delocalized motions of the main chain and of the side chains.

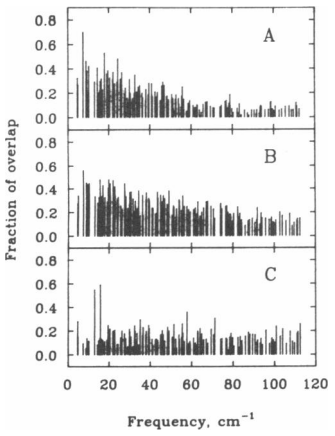

FIGURE 4 Computed fraction of overlap between the exact normal modes and the "ideal" torsion *a*, bending *b*, and stretching *c* modes generated by the continum elastic model for a cylinder. The projections are calculated according to the Eq. 8 in the text. The maximum overlap of a torsional mode occurs at 7.43 cm^{-1} and is equal to 0.7; the maximum overlap of a bending mode occurs at the same frequency and is equal to 0.56; the two peaks in the overlap of the stretching modes are equal to 0.55 and 0.59, and occur at the frequencies 13.0 and 15.8 cm^{-1}, respectively.

To detect and identify such librational motions in the set of normal modes, we generated a subset of 32 hypothetical libration displacement vectors (Lib_i, $i = 1, 32$) consisting of pure amide plane motions. The vectors involved were determined by forcing carbonyl oxygen O_i out of the amide plane, followed by a short energy minimization of C_i, N_{i+1}, and H_{i+1}, during which all other atoms were kept fixed at their original positions; in this way a libration that keeps the amide group approximately planar is generated. The degree of overlap between the subset of 32 amide plane librations and the normal modes is the dot product of the mass-weighted normalized libration vectors ($M^{1/2}$ is the diagonal matrix of the square root of the masses),

$$\mathbf{L}_i = M^{1/2}\,\mathbf{L}_i \tag{9.1}$$

which satisfy the orthogonality condition

$$\mathbf{L}_i \cdot \mathbf{L}_j = \delta_{ij}. \tag{9.2}$$

The total projection of the kth normal mode, $\mathbf{v}_k$, onto the subspace of librational motions is defined by

$$\text{overlap}_k = \left(\sum_{i=1}^{32} (\mathbf{L}_i \cdot \mathbf{v}'_k)^2 \right)^{1/2}. \tag{10}$$

The result of this calculation is shown in Fig. 5. There is a broad band of modes between 75 and 175 cm^{-1} that have a large overlap with the librational motions, although no single mode has an overlap larger than 0.6. Above 200 cm^{-1}, almost no pure librational modes exist (overlap < 0.2). Since 75 cm^{-1} appears to be an upper bound for the collective motions involving the whole dimer, the existence of collective librational motions appears unlikely. This point is considered further when amide plane correlations are discussed.

The librations found here to be in the range 75–175 cm^{-1} are at frequencies significantly lower than the values commonly used in simplified models of the gramicidin-like

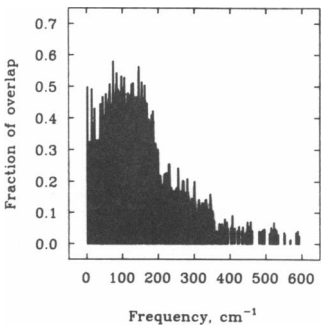

FIGURE 5 Computed fraction of overlap between the exact normal modes and the approximate librational motions of the 32 amide planes. The projections are calculated according to the Eq. 10 in the text.

channel. Fisher and co-workers (24–25) in their study of the influence of channel "softness" on ion selectivity assumed that carbonyl librations were at frequencies between 150 and 550 cm^{-1}; Jordan and co-workers (29) used values in the 200–500 cm^{-1} range; Skerra and Brickmann (31) chose 213 cm^{-1}. Such numerical values are more appropriate for the out-of-plane motion of the oxygen, which is not the dominant mechanism for the C=O dipole reorientation. As shown here it is the lower frequency amide plane librations that are important for reorientation to the carbonyl groups. The fact that the whole transpeptide unit, —NH—CO—, and not just the C=O, is involved in the librational mechanism does not seem to be fully recognized, though it is in accordance with more general treatments of protein dynamics (43, 46).

Backbone Fluctuations

The root mean square (rms) fluctuations at temperature T relative to the minimum energy position given by the harmonic approximation are (45)

$$\langle \Delta \mathbf{R}_i \cdot \Delta \mathbf{R}_i \rangle = k_B T \sum_k (\mathbf{A}_{ik})^2 \frac{1}{\omega_k^2}, \qquad (11)$$

where $\mathbf{A}_{ik}$ is the vector of the projection of the kth normal mode, with frequency ω_k, on the Cartesian components of the displacements vector of the ith atom, $\Delta \mathbf{R}_i$. In the following results, the temperature is taken to be 300°K. To compute the rms fluctuations of any internal coordinate (e.g., a dihedral angle), a corresponding projection and summation is used.

The rms displacements for all backbone atoms are shown in Fig. 6. Only one monomer is shown, since the other one is identical by symmetry. The average rms fluctuation magnitudes are similar for all atoms types (~0.5 Å), with the values of the hydrogen and carbonyl oxygen slightly larger than for the actual main chain atoms. There seems to be a decrease in flexibility toward the middle of the chain and an increase in flexibility at the COOH-terminal end of the molecule and for all atoms, except C^α, at the junction of the two monomers. The larger fluctuations at the junction were noted in a molecular dynamics simulation (32). The fluctuations arise primarily from modes below 75 cm^{-1} (see Fig. 7, *a–d*) with the major contributions coming from modes below 20 cm^{-1} (see Fig.

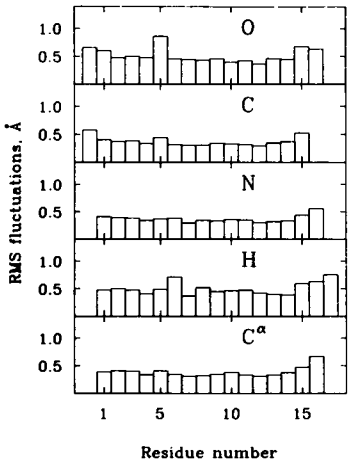

FIGURE 6 Root-mean-square (rms) fluctuations of the backbone atoms of the GA dimer relative to their equilibrium position; atoms (C, H, O, N, C^α) are included. Only one monomer is shown; the other one is identical by symmetry.

7 *e*). Although the larger fluctuations at the ends of the helix are expected, those around L-Ala_5, D-Val_6 are rather surprising. From Fig. 7 *b*, they arise from the larger contribution of the low frequency modes (as compared with Fig. 7 *c*). This part of the chain is hydrogen-bonded to the formyl group of the opposite monomer and could be affected by the flexibility of this group. Also the carbonyl might have large fluctuations due to the fact that the associated NH interacts more weakly with its H-bonded neighbor. The length of most hydrogen bonds do not vary by more than 0.1 Å; this is also the case for four of the six hydrogen bonds in the head-to-head region (see Table III). However, the length of the hydrogen bond between the formyl oxygen and the hydrogen of D-Val_6 varies by 0.2 Å. To determine if this difference arises from the smaller partial charge assigned to the carbon and oxygen of the formyl group, we increased the carbonyl charge of the formyl group from ±0.36 to ±0.55, the value used for peptide carbonyls, and recomputed the frequencies assuming that the normal modes displacements $\mathbf{A}_{i,k}$ are unchanged to first order in the charge pertubation. The perturbed frequencies were computed from the modified second-derivative matrix $\mathbf{V}^*_{ij}$, that is,

$$(\omega_k + \Delta\omega_k)^2 \approx \sum_{ij} \mathbf{A}_{i,k} \mathbf{V}^*_{ij} \mathbf{A}_{j,k}. \qquad (12)$$

The net effect is extremely small, most frequencies changing by <0.5 cm^{-1}. Some crossing of frequencies is observed, due primarily to the fact that many frequencies are nearly degenerate as a result of the dimer symmetry. However, the frequencies below 75 cm^{-1} remained virtually unchanged. Since they constitute the major contribution to the atomic fluctuations (Fig. 7), the latter should not be affected by a change in the formyl partial charges. Thus, it appears that the increase in flexibility at the dimer contact region is caused by the covalent break in the

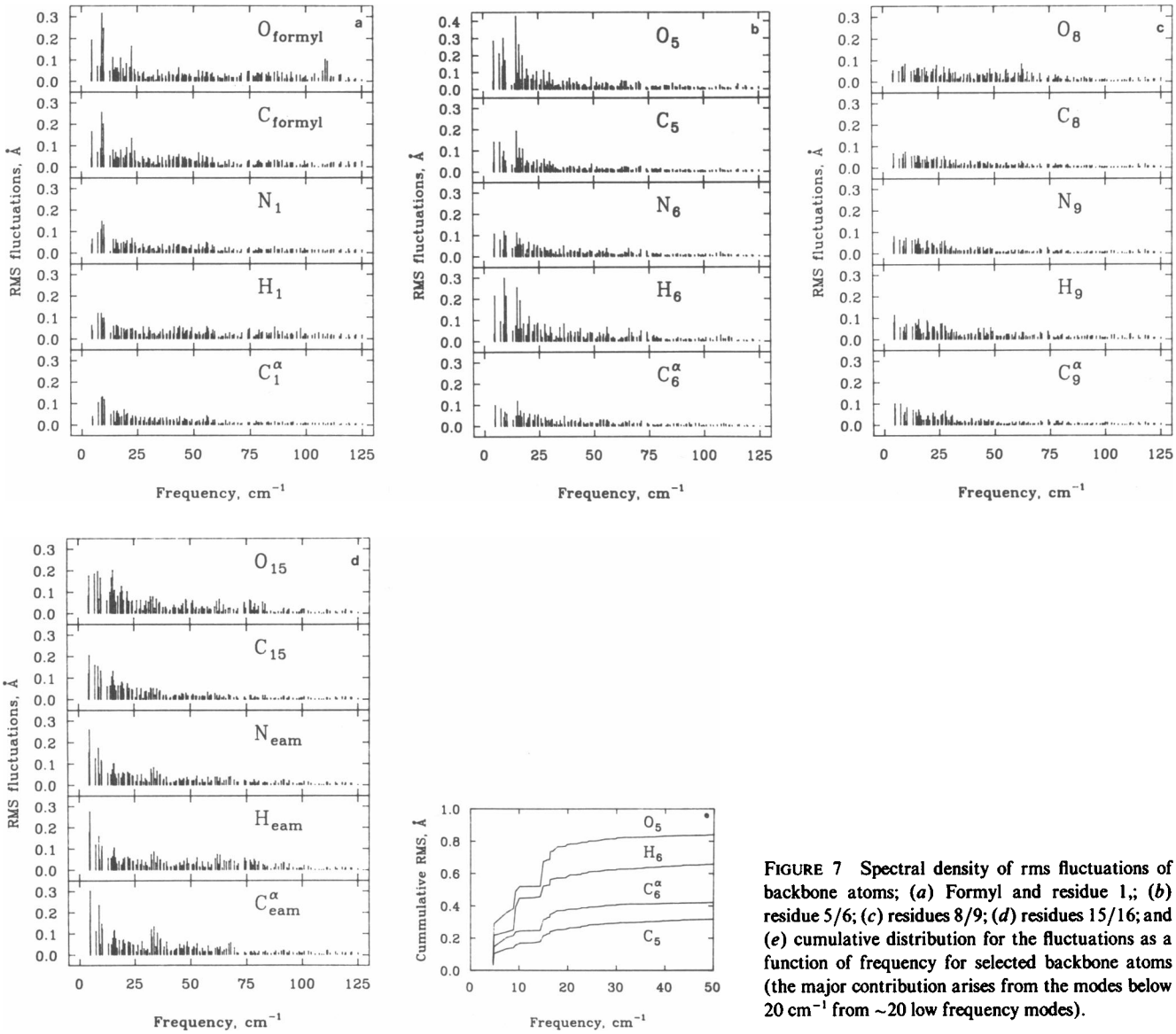

FIGURE 7 Spectral density of rms fluctuations of backbone atoms; (*a*) Formyl and residue 1,; (*b*) residue 5/6; (*c*) residues 8/9; (*d*) residues 15/16; and (*e*) cumulative distribution for the fluctuations as a function of frequency for selected backbone atoms (the major contribution arises from the modes below 20 cm^{-1} from ~20 low frequency modes).

structure of the β helix. The ellipsoid of fluctuation of six carbonyl oxygens is shown in Fig. 8 *a*. It is clear that the large flexibility of oxygens number 3–7 is anisotropic, and oriented radially with regard to the helix axis.

An important feature of the GA dimer is its finite length. At the mouth of the channel, the six last carbonyls (D-Leu$_{10}$ to L-Trp$_{15}$) are H-bonded only to one neighbor, and three "bare" carbonyl oxygens are directly pointing toward the outside of the channel (L-Trp$_{11}$, L-Trp$_{13}$, and L-Trp$_{15}$), as is the hydroxyl group of the ethanol amine tail. The ellipsoid of fluctuation of all backbone atoms at the channel entrance is shown in Fig. 8 *b*. There is an increase in rms fluctuations toward the end of the ethanolamine tail.

Examination of the hydrogen bonds shows significant variation in the length fluctuations (see Table III). The ethanol amine tail-backbone H-bonds and those involving the $C_{1\text{-}7}$ rings show the largest fluctuations.

Dihedral Angle Fluctuations

The rms ϕ-ψ backbone dihedral angles fluctuations are shown in Fig. 9. The average rms angle fluctuation is ~10°, and the largest values are found for ϕ of L-Ala$_5$ and ψ of D-Val$_6$, which is consistent with the above discussion. The fluctuations of the L-amino and D-amino acids do not appear to differ in any systematic way. This finding does not support the conclusion of Venkatachalam and Urry concerning the different role of the L-amino and D-amino acids in the flexibility of GA (40); they suggested that the librational motion of the β-helix involved the simultaneous libration of the all the L-carbonyl or all the D-carbonyl moities. The correlation between the different carbonyls is examined in more detail in the next section.

The rms of the χ_1 and χ_2 side-chain dihedral angle fluctuations are ~10°; the fluctuation in χ_1 is significantly larger for L-Trp$_9$ and L-Trp$_{15}$ (~ 20°).

TABLE III
HYDROGEN BOND ANALYSIS

H-bonds	Length		rms fluctuation
	Before minimization	After minimization	
Inter-monomer H-bonds			
Formyl-O · · ·			
H-D-Val_6	2.60	2.05	0.20
Gly_2-O · · · H-D-Leu_4	3.23	1.89	0.08
Gly_2-H · · · O-D-Leu_4	3.00	1.90	0.09
Intra-monomer H-bonds			
Ala_3-O · · ·			
H-D-Leu_{10}	2.64	1.92	0.09
Ala_3-H · · · O-D-Val_8	2.24	2.93	0.11
Backbone-EAM H-bonds			
EAM-O · · · H-Trp_{11}	4.45	2.06	0.16
EAM-OH · · ·			
O-Trp_{11}	3.86	2.18	0.29
C^{1-7}-like H-bonds			
Trp_9-O · · · H-Trp_{11}	3.43	2.45	0.43
Trp_{11}O · · · H-Trp_{13}	3.43	2.12	0.20
Trp_{13}O · · · H-Trp_{15}	3.43	2.39	0.47

Amide Planes Correlations

To determine whether different amide planes move independently or in a concerted fashion, we consider the equal time correlation factor for the fluctuations of the different ϕ_i-ψ_j dihedral angles, i.e.,

$$C(\Delta\phi_i, \Delta\phi_j) = \frac{\langle \Delta\phi_i \Delta\phi_j \rangle}{\sqrt{\langle \phi_i^2 \rangle \langle \phi_j^2 \rangle}}$$

and similarly for the ψ_i-ψ_j and ϕ_i-ψ_j pairs. Correlation factors for certain dihedral angles are shown in Fig 10, *a–c*. The most striking result is that all ψ angles of the *i*th residues are strongly anticorrelated with the ϕ angles of the $i+1$th residues. This type of correlation has been reported previously in normal mode (45) and molecular dynamics (54) simulations and is indicative of librational motions of the individual amide planes. However, there is no systematic trend in the set of correlation factors. In fact, correlations are small except for structural neighbors that interact due to the hydrogen-bonding pattern and helical conformation of the channel; a case in point is the correlation of ψ_5 with ψ_2 and ψ_{14} with ψ_9.

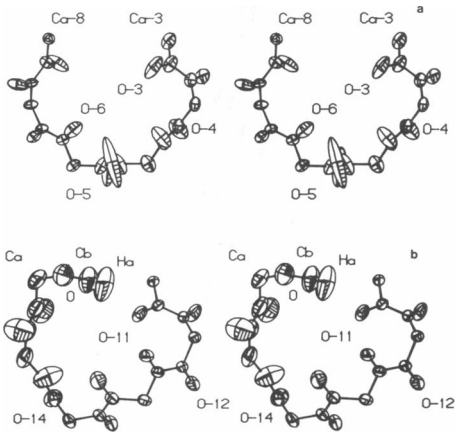

FIGURE 8 CHEMGRAF ellipsoid of fluctuations of backbone atoms. (*a*) Helix strand of six residues located in the middle of the monomer (C_4^α to C_9^α); the fluctuations are significantly anisotropic. (*b*) Helix strand at the channel mouth region (O_{12} to O_{16} plus the OH hydroxyl of the ethanolamine).

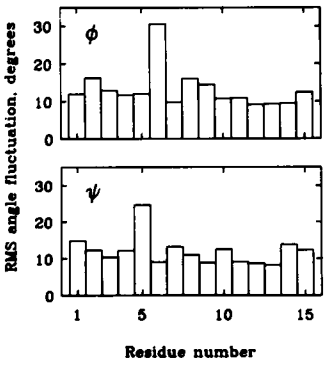

FIGURE 9 Rms fluctuations of the dihedral angles ϕ and ψ as a function of residue number.

To make these structural relations clearer, it is useful to label the amide planes instead of the amino acids themselves; the relabeling is indicated in Table IV. In this notation, the network of hydrogen bonds is represented by a simple diagram (Fig. 11). As an example, we consider amide plane 8 and its nearest neighbors (Fig. 12). One would expect this amide plane to be correlated mostly with 7 and 9, through backbone interactions, and with 2 and 14, through H-bonding interactions. Moreover, the structure of the amide plane should generate anticorrelated librations among H-bonded units, i.e., when the carbonyl oxygen of amide plane 8 moves toward the interior of the channel, a favorable interaction with the hydrogen of amide plane 14 can be retained only if the carbonyl of this plane moves in the opposite direction toward the exterior of the channel. Corresponding correlated motions are expected for all the amide planes.

To test these qualitative arguments, we consider the normalized correlation factor, $C(i, j)$ between the *i*th and *j*th carbonyls. $C(i, j)$ is constructed by introducing $\mathbf{CO}_i(t)$ the instantaneous unit vector associated with the orientation of the *i*th carbonyl at time *t*, i.e.,

$$\mathbf{CO}_i(t) = \frac{\mathbf{R}_{O_i}(t) - \mathbf{R}_{C_i}(t)}{\|\mathbf{R}_{O_i}(t) - \mathbf{R}_{C_i}(t)\|}, \tag{13}$$

where $\mathbf{R}_{C_i}(t)$ and $\mathbf{R}_{O_i}(t)$ are, respectively, the instantaneous position of the *i*th carbonyl carbon and oxygen at time *t*. To first order in the displacements $\Delta\mathbf{R}_{O_i}(t)$ and $\Delta\mathbf{R}_{C_i}(t)$ from their equilibrium positions, we can write

$$\mathbf{CO}_i(t) \approx \mathbf{CO}_{C_i}(\text{eq}) + \mathbf{P}_{i\perp}\left[\frac{\Delta\mathbf{R}_{O_i}(t) - \Delta\mathbf{R}_{C_i}(t)}{R_{CO_i}(\text{eq})}\right], \tag{14}$$

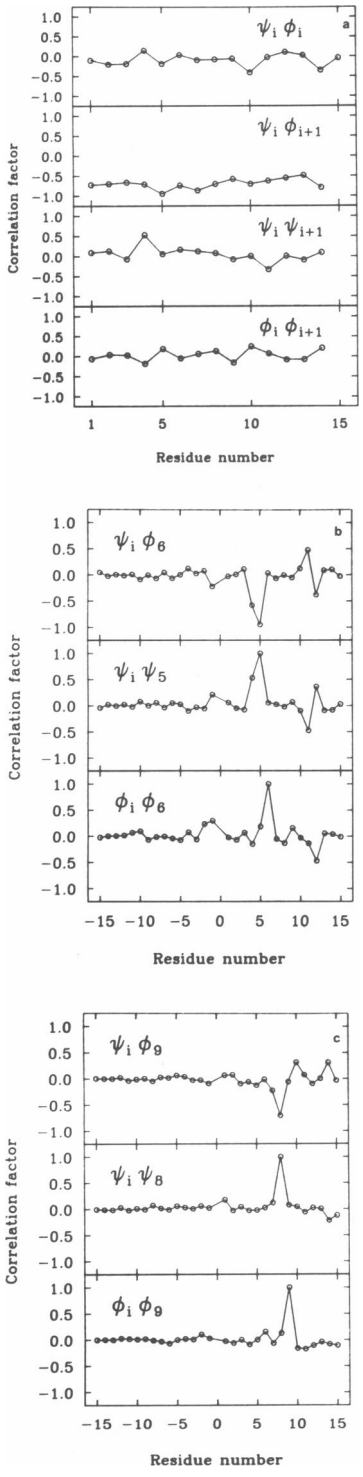

FIGURE 10 Dihedral angles correlations. (*a*) Dihedrals correlation of the backbone connected neighbors. The $\psi_i\,\phi_{i+1}$ correlation is very nearly equal to -1.0; this is associated with the "librational motion" of the amide planes. (*b*) Correlation between dihedral angles associated with amide plane 6 and those of other residues. (*c*) Correlation of dihedral angles associated with amide plane 9 and those of other residues.

TABLE IV
LABELING OF THE AMIDE PLANES*

Amide plane	C, O	N, H
1	CHO	L-Val
2	L-Val	D-Gly
3	D-Gly	L-Ala
4	L-Ala	D-Leu
5	D-Leu	L-Ala
6	L-Ala	D-Val
7	D-Val	L-Val
8	L-Val	D-Val
9	D-Val	L-Trp
10	L-Trp	D-Leu
11	D-Leu	L-Trp
12	L-Trp	D-Leu
13	D-Leu	L-Trp
14	L-Trp	D-Leu
15	D-Leu	L-Trp
16	L-Trp	Eam

*The amide planes of the second monomer are labeled in the same way from -1 to -16.

where $\mathbf{P}_{i\perp}$ is the projector onto a plane perpendicular to $\mathbf{CO}_i(\text{eq})$ and $R_{\text{CO}_i}(\text{eq})$ is the equilibrium distance between C_i and O_i. The fluctuating part of the carbonyl unit vector is then given by

$$\Delta\mathbf{CO}_i(t) \equiv \mathbf{CO}_i(t) - \mathbf{CO}_i(\text{eq}) = \mathbf{P}_{i\perp}\left[\frac{\Delta\mathbf{R}_{\text{O}_i}(t) - \Delta\mathbf{R}_{\text{C}_i}(t)}{R_{\text{CO}_i}(\text{eq})}\right]. \quad (15)$$

This vector was projected onto the cylindrical radial component of the equilibrium position of the ith carbon C_i. A quantity Q_i can then be defined by

$$Q_i = \Delta\mathbf{CO}_i(t) \cdot \mathbf{n}_{\text{C}_i}, \quad (16)$$

where $\mathbf{n}_{\text{C}_i}$ is the ith carbonyl radial unit vector perpendicular to the channel axis. This quantity is positive when the nth carbonyl unit vector moves outward, and negative it moves inward. The normalized correlation factor is then

$$C(i,j) = \frac{\langle Q_i Q_j\rangle}{\sqrt{\langle Q_i^2\rangle\langle Q_j^2\rangle}} \quad (17)$$

with the average in Eq. 17 calculated as a sum over all modes k.

The factor $C(i,j)$ is positive whenever two carbonyls i

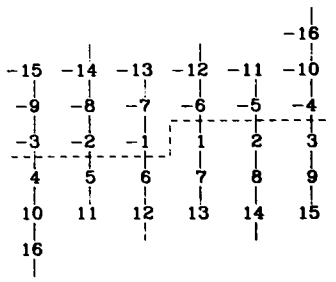

FIGURE 11 Hydrogen bond network pictured by the relabeling of the amide planes; vertical lines indicate the carbonyl oxygen vectors.

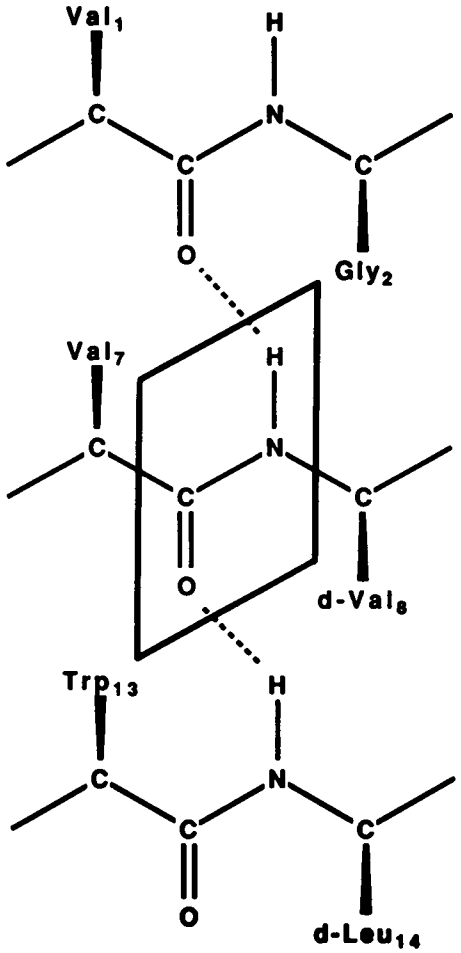

FIGURE 12 Detail of hydrogen bonded amide planes 2-8-14 as described in the text.

and j move in a concerted fashion on the average (i.e., they move inward or outward at the same time; $C(i, j)$ is negative if the motions of two carbonyls are anticorrelated. The correlation matrix is shown as a contour plot diagram in Fig. 13. Each amide plane can be seen to be correlated only with its nearest neighbor in space. There is no significant correlation along the chain. Only anticorrelation is found; most amide planes are anticorrelated with only their first H-bonded neighbors. The flexibility of the main chain dihedral angles, as well as other degrees of freedom does not allow the transmission of the librational state of an amide plane to its more distant neighbors. Along the $(i, i + 6)$ diagonal the correlation factor is significant and negative (-0.2 to -0.4). Although the correlation matrix illustrated in Fig. 13 appears to have the qualitative features of a periodic structure, the $(i, i + 6)$ pattern is not always rigorously maintained. The most negative element is $C(5, 6)$ (-0.5). Correlations are also found to be dominantly negative for $C(i, i + 1)$ though they are not systematic.

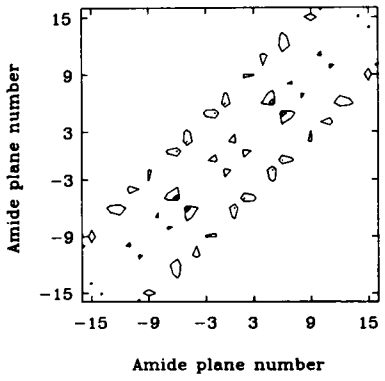

FIGURE 13 Carbonyl dipole correlation matrix $C(i, j)$ as defined by the Eq. 17 in the text. Correlations of -0.2 or less are indicated with contour spaced by 0.05.

The present observations are not in accord with the suggestion made by Venkatachalam and Urry about the existence of long-range correlations between all L- or all D-amino acids librations (40). For a given monomer the carbonyl oxygens of hydrogen-bonded amide planes belong to amino acid of the same chirality. However, their finding of long-range correlations seems to be a spurious effect of the method that they used to determine the librations. By maintaining strict helical symmetry using the Go-Sheraga helix condition (55, 56), they restricted themselves to such correlated motions. In the fully flexible helical structure considered here, the amide planes correlation is limited to one helical turn. The present calculation was performed for a GA in vacuum. Although the presence of water could affect these correlations it is not clear that solvent provides a direct mechanism for enhancing the correlation between adjacent amide planes. Further studies are necessary to clarify this point.

IV. DISCUSSION AND CONCLUSION

The normal mode analysis of GA performed here provides starting point for the study of the flexibility of the channel. Although it uses an approximation to the full potential and solvent was neglected, the lack of error (given the model) and ease of analysis makes normal mode results of considerable interest. The present calculation demonstrates the existence of low frequency amide-plane fluctuations, but do not support the idea of spontaneous correlated carbonyl librations. The rms displacement fluctuations of the carbonyl oxygen appear to be largest in the head-to-head contact region; this result is caused by the break in the covalent helix backbone. The present analysis does not rule out the possibility that significant distortions are induced by the presence of a cation inside the channel. However, such deformations have more to do with the plasticity (ease of deformation) of the GA channel than its elastic (or vibrational) properties. Deformations were observed in a molecular dynamics simulation when a cation was located in the channel (32).

Since an empirical energy function was used in these calculations and hydrogen bonding plays an important structural role in the channel, it is of interest to examine

their effects on the dynamics. The hydrogen bond interaction function in the calculations was based on recent accurate *ab initio* calculations (57). One might expect that making the hydrogen bond weaker would increase carbonyl librations, whereas making them stronger should have an opposite effect. To examine this possibility, we decreased the H-bond interaction by changing the partial charges assigned to all the carbonyl dipoles from ± 0.55 to ±0.44. Using first order perturbation theory, we computed the changes in the frequencies caused by this perturbation. The results showed that most frequencies changed very little and that frequencies below 75 cm^{-1} remained virtually unchanged. Since the low frequency modes are dominant in the rms fluctuations, the present results concerning the flexibility of the GA dimer appear to depend only weakly on the strength of the hydrogen bonds. This is in accord with earlier work on an α-helix (45) where only the overall stretching modes were sensitive to the strength of the hydrogen bonds.

The carbonyl–carbonyl correlation matrix shows that most of the amide planes are only weakly correlated, and that only hydrogen-bonded neighbors are significantly anticorrelated. This observation, combined with the fact that collective modes have frequencies below 75 cm^{-1} and that "carbonyl librations" are located in the band going between 75 to 175 cm^{-1} rule out the possibility of collective librational motions extending along a significant portion of the structure. The GA helix does not sustain such correlated motions due to the inherent flexibility of the helical structure. Again, we emphasize that these results apply to the spontaneous vibrations of an empty GA, and do not rule out the possibility of larger structural changes in presence of an ion.

The present results for the gramicidin channel in vacuum and in the absence of ions make clear that it is a very flexible system. Although GA does not sustain correlated fluctuations, it is likely that distortions and changes in dynamic properties due to the presence of ions, as modulated by solvent, will play an important role in the permeability. Full energy minimization of the channel in presence of a sodium ion indicates that important structural changes do take place (Roux, B., and M. Karplus, unpublished calculations). Macroscopic properties, such as the channel length, as well as localized features, such as carbonyl orientations, appear to be affected. Further, perturbation calculations in the presence of a sodium ion show that there are large changes in the vibrational frequencies. Given the flexibility of the system, the use of a rigid (33–38) or nearly rigid (23–31) gramicidin channel is not an appropriate approximation of the system. Future work will be directed toward obtaining a deeper understanding of the role of flexibility in the properties of the gramicidin channel.

This paper was supported in part by a grant from the National Science Foundation.

Received for publication 16 July 1987 and in final form 22 October 1987.

REFERENCES

1. Andersen, O. S. 1984. Gramicidin channels. *Annu. Rev. Physiol.* 46:531–548.
2. Fisher, R., and T. Blumenthal. 1982. An interaction between gramicidin and the σ subunit of RNA polymerase. *Proc. Natl. Acad. Sci. USA.* 79:1045–1048.
3. Finkelstein, A., and O. S. Andersen. 1981. The Gramicidin channel: a review of its permeability characteristics with special reference to the single-file aspect of transport. *J. Membr. Biol.* 59:155–171.
4. Wallace, B. A. 1986. Structure of gramicidin A. *Biophys. J.* 49:295–306.
5. Koeppe, R. E., II, J. H. Berg, K. O. Hodgson, and L. Stryer. 1979. Gramicidin A crystals contain two cation binding sites per channel. *Nature (Lond.).* 279:723–725.
6. Koeppe, R. E., II, K. O. Hodgson, and L. Stryer. 1978. Helical channels in crystals of gramicidin A and of a cesium-gramicidin A complex: an x-ray diffraction study. *J. Mol. Biol.* 121:41–54.
7. Urry, D. W. 1971. The gramicidin A transmembrane channel: a proposed $\pi_{(L,D)}$ helix. *Proc. Natl. Acad. Sci. USA.* 68:672–676.
8. Naik, V. M., and S. Krimm. 1986. Vibrational analysis of the structure of gramicidin A. I. Normal mode analysis. *Biophys. J.* 49:1131–1145.
9. Naik, V. M., and S. Krimm. 1986. Vibrational analysis of the structure of gramicidin A. II. Normal mode analysis. *Biophys. J.* 49:1147–1151.
10. Boni, L. T., A. J. Connolly, and A. M. Kleinfeld. 1986. Transmembrane distribution of gramicidin by tryptophane energy transfer. *Biophys. J.* 49:122–123.
11. Durkin, J. T., O. S. Andersen, E. R. Blout, F. Heitz, R. E. Koeppe II, and Y. Trudelle. 1986. Structural information from functional measurements: single-channel studies on gramicidin analogues. *Biophys. J.* 49:118–121.
12. Koeppe, R. E., II, and B. P. Schoenborn. 1984. 5-Å Fourier map of gramicidin A phased by deuterium-hydrogen solvent difference neutron diffraction. *Biophys. J.* 45:503–507.
13. Urry, D. W., C. M. Venkatachalam, A. Spisni, P. Laüger, and M. A. Khaled. 1980. Rate theory calculations of gramicidin single-channel currents using NMR-derived rate constants. *Proc. Natl. Acad. Sci. USA.* 77:2028–2032.
14. Urry, D. W., K. U. Prasad, and T. L. Trapane. 1982. Location of monovalent cation binding sites in the gramicidin channel. *Proc. Natl. Acad. Sci. USA.* 79:390–394.
15. Urry, D. W., J. T. Walker, and T. L. Trapane. 1982. Ion interactions in (1-supl3C)C-Val[8] and D-Leu[14] analogs of gramicidin A, the Helix sense of the channel and location of ion binding sites. *J. Membr. Biol.* 69:225–231.
16. Urry, D. W., T. L. Trapane, J. T. Walker, and K. U. Prasad. 1982. On the relative lipid membrane permeability of Na^+ and Ca^{2+}. A physical basis for the messenger role of Ca^{2+}. *J. Biol. Chem.* 257:6659–6661.
17. Smith, R., and B. A. Cornell. 1986. Dynamics of the intrinsic membrane polypeptide gramicidin A in phospholipid bilayers. A solid-state ^{13}C nuclear magnetic resonance study. *Biophys. J.* 49:117–118.
18. Arseniev, A. S., V. F. Bystrov, V. T. Ivanov, and Yu. A. Ovchinnikov. 1984. NMR solution conformation of gramicidin A double helix. *FEBS (Fed. Eur. Biochem. Soc.).* 165:51–56.
19. Arseniev, A. S., I. L. Barsukov, V. F. Bystrov, A. L. Lomize, and Yu. A. Ovchinnikov. 1985. ^1H-NMR study of gramicidin A transmembrane ion channel. Head-to-head right-handed, single-stranded helices. *FEBS (Fed. Eur. Biochem. Soc.) Lett.* 186:168–174.
20. Weinstein, S., B. A. Wallace, J. S. Morrow, and W. R. Veatch. 1980. Conformation of the gramicidin A transmembrane channel: a ^{13}C

nuclear magnetic resonance study of ^{13}C-enriched gramicidin in phosphatidylcholine vesicles. *J. Mol. Biol.* 143:1–19.
21. Läuger, P. 1973. Ion transport through pores: a rate-theory analysis. *Biochim. Biophys. Acta.* 311:423–441.
22. Läuger, P. 1982. Microscopic calculation of ion-transport rates in membrane channels. *Biophys. Chem.* 15:89–100.
23. Fisher, W., J. Brickmann, and P. Läuger. 1981. Molecular dynamics study of ion transport in transmembrane protein channels. *Biophys. Chem.* 13:105–116.
24. Fisher, W., and J. Brickmann. 1983. Ion-specific diffusion rates through transmembrane protein channels. A molecular study. *Biophys. Chem.* 18:323–337.
25. Cooper, K., E. Jakobsson, and P. Wolynes. 1985. The theory of ion transport through membrane channels. *Prog. Biophys. Biol.* 46:51–96.
26. Schröder, H. 1985. Rate theoretical analysis of ion-selectivity in membrane channels with elastically bound ligand. *Eur. Biophys. J.* 12:129–142.
27. Polymeropoulos, E. E., Brickmann, J. 1985. *Ann. Rev. Biophys. Chem.* 14:315–330.
28. Lee, W. K., and P. C. Jordan. 1984. Molecular dynamics simulation of cation motion in water-filled gramicidinlike pores. *Biophys. J.* 46:805–819.
29. Sung, S., and P. C. Jordan. 1987. Why is gramicidin valence selective? *Biophys. J.* 51:661–672.
30. Vertenstein, M., and D. Ronis. 1986. Microscopic theory of membrane transport. *J. Chem. Phys.* 85:1628–1649.
31. Skerra, A., and J. Brickmann. 1987. Structure and dynamics of one-dimensional ionic solutions in biological transmembrane channels. *Biophys. J.* 51:969–976.
32. Mackay, D. H. J., P. H. Berens, K. R. Wilson, and A. T. Hagler. 1983. Structure and dynamics of ion transport through gramicidin-A. *Biophys. J.* 46:229–248.
33. Pullman, A., and C. Etchebest. 1983. The gramicidin A channel: the energy profile for single and double occupancy in a head-to-head $\beta^{6,3}_{3,3}$-helical dimer backbone. *FEBS (Fed. Eur. Biochem. Soc.) Lett.* 163:199–202.
34. Etchebest, C., S. Ranganathan, and A. Pullman. 1984. The gramicidin A channel: comparison of the energy profiles of Na^+, K^+, and Cs^+. *FEBS (Fed. Eur. Biochem. Soc.) Lett.* 173:301–306.
35. Etchebest, C., and A. Pullman. 1986. The gramicidin A channel: energetics and structural characteristics of the progression of a sodium ion in the presence of water. *J. Biomol. Struct. & Dyn.* 4:805–825.
36. Etchebest, C., and A. Pullman. 1986. The energy profile for Na^+ in the presence of water with inclusion of the flexibility of the ethanolamine tail. *FEBS (Fed. Eur. Biochem. Soc.) Lett.* 204:261–265.
37. Kim, K. S., and E. Clementi. 1985. Energetics and hydration structures of a solvated gramicidin A transmembrane channel for K^+ and Na^+ cations. *J. Am. Chem. Soc.* 107:5504–5513.
38. Kim, K. S., D. P. Vercauteren, M. Welti, S. Chin, and E. Clementi. 1985. Interaction of K^+ ion with the solvated gramicidin A transmembrane channel. *Biophys. J.* 47:327–335.
39. Venkatachalam, C. M., and D. W. Urry. 1983. Theoretical conformational analysis of the gramicidin A transmembrane channel. I. Helix sense and energetics of head-to-head dimerization. *J. Comp. Chem.* 4:461–469.
40. Venkatachalam, C. M., and D. W. Urry. 1983. Theoretical analysis of gramicidin A transmembrane channel. II. Energetics of helical librational states of the channel. *J. Comp. Chem.* 5:64–71.
41. Koeppe, R. E., II, and M. Kimura. 1984. Computer building of β-helical polypeptide models. *Biopolymers.* 23:23–38.
42. Urry, D. W., C. M. Venkatachalam, K. U. Prasad, R. J. Bradley, G. Parenti-Castelli, and G. Lenaz. 1981. Conductance process of the gramicidin channel. *Int. J. Quantum Chem. Symp.* 8:385–399.
43. Karplus, M., and J. A. McCammon. 1983. Dynamics of proteins: elements and function. *Annu. Rev. Biochem.* 53:263–300.
44. Levy, R. M., D. Perahia, and M. Karplus. 1982. Molecular dynamics of an α-helical polypeptide: temperature dependence and deviation from harmonic behavior. *Proc. Natl. Acad. Sci. USA.* 79:1346–1350.
45. Levy, R. M., and M. Karplus. 1979. Vibrational approach to the dynamics of an α-helix. *Biopolymers.* 18:2465–2495.
46. Brooks, B., and M. Karplus. 1983. Harmonic dynamics of proteins: normal modes and fluctuations in bovine pancreatic trypsin inhibitor. *Proc. Natl. Acad. Sci. USA.* 80:6571–6575.
47. Kuriyan, J., G. A. Petsko, R. M. Levy, and M. Karplus. 1986. Effect of anisotropy and anharmonicity on protein crystallographic refinement: an evaluation by molecular dynamics. *J. Mol. Biol.* 190:227–254.
48. Brooks, B. R., R. E. Bruccoleri, B. D. Olafson, D. J. States, S. Swaminathan, and M. Karplus. 1983. CHARMM: a program for macromolecular energy, minimization, and dynamics calculations. *J. Comp. Chem.* 4:187–217.
49. Pettitt, B. M., and M. Karplus. 1985. The potential of mean force surface for the alanine dipeptide in aqueous solution: a theoretical approach. *Chem. Phys. Lett.* 121:194–201.
50. Go, N., T. Noguti, and T. Nishikawa. 1983. Dynamics of a small globular protein in terms of low-frequency vibrational modes. *Proc. Natl. Acad. Sci. USA.* 80:3696–3700.
51. Levitt, M., C. Sander, and P. S. Stern. 1985. Protein normal-mode dynamics: trypsin inhibitor, crambin, ribonuclease, and lysozyme. *J. Mol. Biol.* 181:423–447.
52. Elber, R., and M. Karplus. 1986. Low-frequency modes in proteins: Use of the effective-medium approximation to interpret the fractal dimension observed in electron-spin relaxation measurements. *Phys. Rev. Lett.* 56:394.
53. Malvern, L. E. 1969. Introduction to the Mechanics of a Continuous Media. Prentice-Hall Inc., Englewood Cliffs, NJ.
54. McCammon, J. A., B. R. Gelin, and M. Karplus. 1977. Dynamics of folded proteins. *Nature (Lond.).* 267:585–590.
55. Go, N., and H. A. Scheraga. 1973. Ring closure in chain molecules with Cn, I, or S_{2n} symmetry. *Macromolecules.* 6:273.
56. Go, N., and A. Okuyama. 1976. A method for calculating dihedral angles in helical polymers with given values of unit height and unit rotation. *Macromolecules.* 9:867.
57. Reiher, W. 1986. Theoretical Studies of Hydrogen Bonding. Ph. D. thesis. Chemistry, Harvard University, Cambridge, MA.
58. Weiner, S. J., P. A. Kollman, D. A. Case, U. C. Singh, C. Ghio, G. Alagona, S. Profera, Jr., and P. Weiner. 1984. A new force field for molecular mechanical simulation of nucleic acid and proteins. *J. Am.* 106:765.